Chain Stiffness and Attachment-Dependent Attraction between Polyelectrolyte-Grafted Colloids

Gaurav Arya*

Department of NanoEngineering, 9500 Gilman Drive, Mail Code 0448, University of California, San Diego, La Jolla, California 92093, United States

Received: March 31, 2010; Revised Manuscript Received: October 17, 2010

We report here the effects of chain stiffness and surface attachment on the effective interactions between polyelectrolyte-grafted colloidal particles in monovalent salt obtained using Monte Carlo simulations. Our approach involves computation of the distance-dependent potential of mean force between two polyelectrolyte-grafted colloidal particles treated at a coarse-grained resolution. Two chain stiffnesses, flexible and stiff, and two surface attachment modes, free and constrained, at low grafting densities are examined. PMF calculations across a range of surface and polyelectrolyte charge allows us to map out the strength and extent of the attractive and repulsive regime in the two-dimensional charge space. We observe striking differences in the effects of chain stiffness between the two modes of attachment. When the chains are freely attached, the stiff-chains colloids exhibit a marginal reduction in the attraction compared to their flexible-chain counterparts. In contrast, when the chains are attached in a constrained manner, the colloids with stiff chains exhibit a significantly stronger attraction and a broader attractive regime compared to flexible-chain colloids. These differences in the effects of stiffness between the two attachment modes are explained in terms of differences in the energetic and entropic forces balancing adsorption of chains at their own surface versus chain extension to mediate bridging interactions across two particles. Our results thus underscore the importance of surface attachment of chains and its proper accounting in computational and experimental studies and suggests the mode of chain attachment as an additional control parameter for modulating intercolloid interactions for applications such as stabilization of colloidal systems and bottom-up self-assembly of nanostructures.

1. Introduction

Studying the interactions between polyelectrolyte-grafted colloids where the polyelectrolyte chains carry charges opposite in sign to those carried by the surfaces is important from both a fundamental and industrial perspective. Such interactions are understandably more complex than those between uncharged colloids grafted with neutral polymers[1,2] due to the introduction of electrostatic forces into the system that can have both repulsive and attractive effects. Under conditions of low surface grafting density, sufficiently short chains, and similar surface and polyelectrolyte charge magnitudes, two such colloidal particles can experience an effective attraction despite the net charge carried by the particle being nonzero, giving rise to the so-called "like-charge attraction" phenomenon.[3−5]

Several theoretical studies comprised of mean field approaches[6−13] and molecular simulations[12−19] have investigated the origin of this attraction. It is now well understood that polymer-bridging interactions[3,4,18] and charge−charge correlations[17,20] are the two main sources of the attraction. The former effect arises from the adsorption of chains from one particle to the surface of another, causing the formation of an attractive bridge between the two particles. Such bridging is not only energetically favorable but also favorable from an entropic point of view.[5] The latter arises from correlations between the position of the charged chains without any actual bridging; in fact, the charge correlation effect may be the strongest when the chains are strongly adsorbed at their own colloid surface and not bridging to the surface of another colloid.[17] Due to the large number of parameters, a comprehensive understanding of the interactions between polyelectrolyte-grafted colloids is still lacking. While the effects of some parameters such as the surface and polyelectrolyte charges, temperature, and salt concentration have been delineated to some extent, the effect of other parameters such as the stiffness of the chains and their method of attachment have not been studied so far.

The effect of chain stiffness on the interactions colloids is quite straighforward in the case of uncharged hard spheres grafted with neutral polymers, where an increase in chain stiffness leads to a stronger repulsion between the particles due to steric overlap among the polymer chains. However, the presence of charges complicates this situation, as the chain conformations now become strongly dependent on the magnitude of the surface and polyelectrolyte charges. We anticipate a charge and chain stiffness dependent competition between chains adsorbing onto their own colloidal surface or extending outward to mediate polymer-bridging interactions across two colloidal surfaces. Furthermore, the manner in which the chains are attached to the colloid surface could also critically affect their configurations and the balance between their surface adsorbed and extended states. Consequently, chains that are attached in a "free" manner, where they are free to emerge at any angle relative to the surface, may possess a larger propensity to collapse at their surface compared to chains that are attached in a "constrained" manner, where they are forced to emerge normal to the surface due to the particular grafting approach utilized.[21] Such issues related to the chain stiffness and attachment need to be resolved in order to develop a more complete understanding of polyelectrolyte-grafted colloids.

* To whom correspondence should be addressed. E-mail: garya@ucsd.edu. Phone: 858-822-5542. Fax: 858-534-9553.

10.1021/jp1029085
Published on Web 11/11/2010

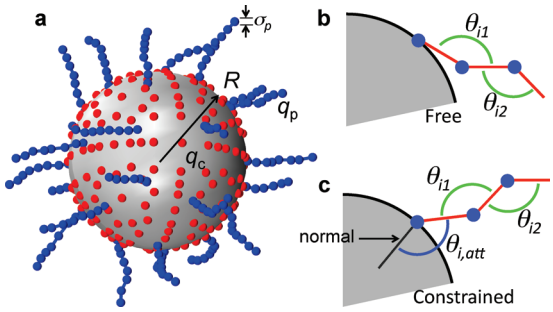

Figure 1. (a) Coarse-grained model of a polyelectrolyte-grafted colloidal particle employed in this study. The polyelectrolyte beads and surface charges are shown in blue and red, respectively. The excluded volumes of the charges are not drawn to scale. Two types of surface attachments are considered: (b) free, where chains emerge from the surface without any constraint on their exit angle, and (c) constrained, where chains prefer to emerge normal to the surface due to an additional harmonic constraint on the exit angle. Angle constraints for regular bonds and the exit angle are depicted by the black and green arcs.

In this study, we investigate for the first time the impact of chain stiffness and their attachment mode on the interactions between polyelectrolyte-grafted colloids using Monte Carlo simulations. Our approach involves exhaustive computation of the potential of mean forces between the colloids as a function of chain stiffness, attachment, and surface and polyelectrolyte charges. We find that the chain stiffness can have drastically different effects on the strength of attraction between the colloids, depending on the manner in which the chains are attached to the surface, decreasing in the case of freely attached chains and surprisingly increasing in the case of constrained chains. A detailed analyses of the free energy components reveals intriguing mechanisms behind these effects. Our study thus emphasizes the importance of correctly accounting for the attachment of polyelectrolytes to charged surfaces and proposes the attachment method as an additional control parameter for tuning interactions between colloids.

2. Methods

2.1. Coarse-Grained Model of Colloids. The polyelectrolyte-grafted colloids are treated using the coarse-grained representation introduced in our previous study[5] (Figure 1a). The colloid is treated as a sphere of radius $R = 10$ nm carrying $n_c = 250$ fixed charged beads scattered uniformly on the surface using the Marsaglia algorithm,[22] each carrying a charge $q_c > 0$. The colloid is grafted with $n_p = 26$ polyelectrolyte chains treated as bead chains comprising $N = 8$ coarse-grained beads, each carrying a charge $q_p < 0$. The equilibrium length of each polymer chain is 8 nm, and the grafting density is ~0.02 chains/nm^2. Choosing 250 surface charges provides a good balance between computational costs and a smooth representation of the colloid surface. Choosing 26 chains allows us to connect them equidistant from each other on the colloid surface to yield an isotropic colloid. Each surface charge is assigned an excluded volume potential that prevents other colloids and their chains from penetrating the colloid surface. Our colloids thus represent nanoparticles grafted with short polymers at a low grafting density.[23,24] The chain lengths and grafting density ensure that the steric repulsion between colloidal particles does not dominate the attractive forces.

The chains are assigned an intramolecular force field comprised of harmonic stretching and bending terms, and the total intramolecular energy is given by

$$U_{\text{chain}} = \sum_i \left(\sum_{j=1}^{N-1} k_s (l_{ij} - l_0)^2 + \sum_{j=1}^{N-2} k_\theta (\theta_{ij} - \theta_0)^2 \right) \quad (1)$$

where the sum i runs over all chains, k_s and k_θ are the stretching and bending constants, respectively, l_{ij} is the bond length between beads j and $j + 1$ of chain i, θ_i is the bond angle between beads j, $j + 1$, and $j + 2$ of chain i, and l_0 and θ_0 are the equilibrium bond lengths and angles. The equilibrium bond lengths are fixed to $l_0 = 1$ nm, and bond angles are fixed to 180°. A stiff bond constant of $k_s = 10$ kcal/mol/nm^2 ensures that the bonds remain quite rigid. We also employ two chain stiffnesses: *flexible* with $k_\theta = 0.1$ kcal/mol/rad^2 and *stiff* with $k_\theta = 10$ kcal/mol/rad^2 to represent two extreme configurations of the chains, random coil and extended.

A key aspect of this study is the consideration of two different chain attachment modes representing two limiting ways by which polymer chains are attached to surfaces. In one mode, the chains are attached at defined fixed points $\mathbf{r}_{i0}$ (where i represents the chain index) on the colloid surface using a strong harmonic spring (Figure 1b). Because there is no constraint on the orientation of the chain as it emerges from the surface, this attachment mode is termed "free". The total attachment energy of all free chains is given by

$$U_{\text{att,free}} = \sum_i k_{s,\text{att}} |\mathbf{r}_{i1} - \mathbf{r}_{i0}|^2 \quad (2)$$

where index i runs over all chains, $\mathbf{r}_{i1}$ is the position of the bead attached to the surface, and $k_{s,\text{att}} = 10$ kcal/mol/nm^2 is the stiffness of the harmonic spring used for the attachment. Such freely attached chains could in reality represent chains grafted (covalently linked) to the surface via flexible or dangling functional groups that do not constrain the chains to emerge at any particular orientation relative to the surface.[21]

We also consider a second attachment mode, which we term "constrained". Here, in addition to the harmonic spring attaching the chains to the colloid, there also exists a constraint on the angle subtended by the chain and the surface such that chains prefer to emerge normally from the colloid surface. To implement this constraint, we add a harmonic bending energy term for the angle formed by the colloidal particle, the attachment bead, and the next bead in the chain with an equilibrium angle of 180° (Figure 1c). The total attachment energy for all constrained chains is then given by

$$U_{\text{att,const}} = \sum_i \left(k_{s,\text{att}} |\mathbf{r}_{i1} - \mathbf{r}_{i0}|^2 + k_{\theta,\text{att}} (\theta_{i,\text{att}} - \pi)^2 \right) \quad (3)$$

where $k_{\theta,\text{att}} = 10$ kcal/mol/rad^2 is the bending rigidity of the constraint and $\theta_{i,\text{att}}$ is the angle subtended by the center of the colloid, the attached bead, and the second bead. These constrained chains could, for instance, represent chains attached to surfaces via elevated and/or rigid, bulky functional groups that constrain the chains to emerge at an angle normal to the surface.[21] It is also likely that such "grafted-to" approaches could constrain the chains to emerge at other angles and that chains physisorbed on the surface (not covalently attached) could predispose the chains to emerge parallel to the surface. In this study we consider only the normal orientation constraint.

TABLE 1: Parameter Values for the Coarse-Grained Model of Colloid

parameter	description	value
R	radius of colloid	10 nm
n_p	number of polyelectrolyte chains attached to core	26
N	number of beads composing each polyelectrolyte chain	8
n_c	number of charges on colloid surface	250
l_0	equilibrium segment length of polymer	1 nm
θ_0	equilibrium angle between three chain beads	180°
k_s	stretching constant of chains	10 kcal/mol/nm^2
$k_{s,att}$	stretching constant of harmonic spring used attaching chains	10 kcal/mol/nm^2
k_θ	bending constant of flexible chains	0.1 kcal/mol/rad^2
	bending constant of stiff chains	10 kcal/mol/rad^2
$k_{\theta,att}$	bending constant for exit angle constraint	10 kcal/mol/rad^2
ε	LJ energy parameter for all excluded volume interactions	0.1 kcal/mol
σ_{cc}	LJ size parameter for surface charge interactions	1.2 nm
σ_{cp}	LJ size parameter for chain bead/surface charge interactions	1.8 nm
σ_{pp}	LJ size parameter for chain bead interactions	1.8 nm
ε	dielectric constant of solvent	80
c_s	electrolyte concentration	22 mM
κ	inverse Debye length	0.5 nm^{-1}
T	temperature	293.15 K

The colloid charges and polyelectrolyte beads are assigned an excluded volume using the Lennard-Jones potential. The total excluded volume energy is therefore given by

$$U_{\text{excl}} = \sum_{i,j>i} 4\varepsilon_{ij}\left[\left(\frac{\sigma_{ij}}{r_{ij}}\right)^{12} - \left(\frac{\sigma_{ij}}{r_{ij}}\right)^{6}\right] \tag{4}$$

where the sum i, j runs over all charges (surface charges plus polyelectrolyte beads) and σ_{ij} is the size parameter and ε_{ij} the well-depth of the potential. We assign $\sigma_{cc} = 1.2$ nm, $\sigma_{pp} = 1.8$ nm, and $\sigma_{cp} = 1.8$ nm for interactions between surface charges, between chain beads, and between surface charges and chain beads, respectively. These parameters were chosen to ensure that the polyelectrolyte chains cannot penetrate the colloid surface and to also ensure that the chain/surface electrostatic interactions do not become excessively strong that sampling becomes problematic. The energy parameter $\varepsilon_{ij} = 0.1$ kcal/mol was kept small ($\ll k_BT$) such that it does not affect the attraction between the two colloidal particles and also does not affect chain conformations; i.e., the solvent quality remains roughly neutral (theta-like). Using purely repulsive or hard-sphere potentials for the excluded volume interactions should have negligible effect on the results.

We consider the colloids to be present in a 1:1 electrolyte (monovalent salt). Therefore, screened electrostatic interactions between all charges in the system are treated using the Debye−Hückel potential,[25] and the total electrostatic energy of the colloids is given by

$$U_{\text{elec}} = \sum_{i,j>i} \frac{q_i q_j}{4\pi\varepsilon\varepsilon_0 r_{ij}} \exp(-\kappa r_{ij}) \tag{5}$$

where the sum i, j runs over all charge pairs, q_i and q_j are separated by a distance r_{ij}, ε_0 is the permittivity of vacuum, and ε is the dielectric constant of water. The inverse Debye length κ is given by $(2e^2c_s/\varepsilon\varepsilon_0k_BT)^{1/2}$, where e is the electronic charge, k_B is the Boltzmann constant, T is the temperature, and c_s is the salt concentration. The temperature is fixed at 20 °C and salt concentration c_s at 22 mM to yield a Debye length of ~2 nm, which is smaller than the chain length but longer than the excluded size of the surface charges and chain beads.

The charges on the same surface do not interact with each other via both excluded volume and Debye−Hückel potentials, and therefore their interactions do not contribute to the total energy. Similarly, beads on the same chain i and j closer than three beads ($j - i < 3$) do not interact with each other, as they are already constrained by the harmonic bond and bending angle potentials. Additionally, to save computational costs, we employ distance cutoffs for both types of potentials: 4 nm for excluded volume interactions and 15 nm for electrostatic interactions.

The total energy of interaction of two colloidal particles, U_{tot}, is therefore given by the sum of electrostatic, excluded volume, intramolecular, and surface-attachment energies

$$U_{\text{tot}} = U_{\text{elec}} + U_{\text{excl}} + U_{\text{chain}} + U_{\text{att},k} \tag{6}$$

where k refers to either a constrained or a free attachment mode. The force field parameters used in this study are also listed in Table 1.

2.2. Potential of Mean Force Calculations. The potential of mean force (PMF) between two polyelectrolyte-grafted colloids separated by a center-to-center distance d is computed from the average force $\langle F(d)\rangle$[26] experienced by the particles in the direction along the particle centers, suitably averaged over all configurational degrees of freedom

$$\langle F(d)\rangle = \frac{\int\cdots\int -\left(\frac{\partial U_{\text{tot}}(d,\mathbf{\Omega})}{\partial d}\right)\exp(-U_{\text{tot}}(d,\mathbf{\Omega})/k_BT)\,d\mathbf{\Omega}}{\int\cdots\int \exp(-U_{\text{tot}}(d,\mathbf{\Omega})/k_BT)\,d\mathbf{\Omega}} \tag{7}$$

where U_{tot} is the total energy computed using eqs 1−6, and the integral is computed over all degrees of freedom (colloid rotation and chain configurations) denoted by $\mathbf{\Omega}$. To compute the right-hand side of eq 7, we generate Boltzmann distributed configurations of the two colloids for each separation distance d using Monte Carlo (MC) simulations.

Our MC simulations are comprised of two moves: rotation and chain regrowth. In the rotation move, one of the two particles is randomly chosen and the entire particle including the grafted chains is rotated by a random angle $\Delta\theta$ sampled from a uniform distribution $-45° < \Delta\theta < 45°$ about a randomly

chosen axis. The move is accepted using the Metropolis acceptance criterion[27]

$$p_{acc} = \min[1, \exp(-\Delta U_{tot}/k_B T)] \quad (8)$$

where ΔU_{tot} is the change in the total energy upon rotation. In the regrowth move, a polyelectrolyte chain is randomly chosen and regrown from scratch using the configurational bias MC approach.[28−30] The regrown chain is then accepted with the Rosenbluth acceptance criterion

$$p_{acc} = \min\left[1, \frac{W_{new}}{W_{old}}\right] \quad (9)$$

where W_{old} and W_{new} are the Rosenbluth weights of the original and regrown chain, respectively.

The PMF, which we denote by $\mathcal{A}(d)$ due to its resemblance to the Helmholtz free energy, is computed by integrating the computed average force:[26]

$$\mathcal{A}(d) = -\int_{\infty}^{d} \langle F(\xi)\rangle \, d\xi \quad (10)$$

The free energy $\mathcal{A}(d)$ can be further decomposed into its energetic and entropic components to determine their contribution to the total free energy. The energetic component (d) can be determined from the same MC simulation, as given by

$$\mathcal{U}(d) \equiv \langle U_{tot}(d)\rangle = \frac{\int \cdots \int U_{tot}(d, \mathbf{\Omega}) \exp(-U_{tot}(d, \mathbf{\Omega})/k_B T) \, d\mathbf{\Omega}}{\int \cdots \int \exp(-U_{tot}(d, \mathbf{\Omega})/k_B T) \, d\mathbf{\Omega}} \quad (11)$$

while the entropic contribution $\mathcal{S}(d)$ can be computed using the thermodynamic relation

$$\mathcal{S}(d) = \frac{\mathcal{U}(d) - \mathcal{A}(d)}{T} \quad (12)$$

The above methodology provides a convenient route toward obtaining the energetic and entropic driving forces for the observed interactions between polyelectrolyte-grafted colloids.

2.3. Colloidal Systems and Conditions Investigated. We study four different colloidal systems constituted from the combination two chain stiffnesses and two modes of attachment introduced earlier: (i) *free, flexible*, colloids with flexible chains attached with a harmonic spring but without any exit angle constraints; (ii) *free, stiff*, colloids with stiff chains attached with a harmonic spring but without any exit angle constraints; (iii) *constrained, flexible*, colloids with flexible chains attached with an exit angle constraint in addition to a harmonic spring such that the chains prefer to emerge normally from the surface; and (iv) *constrained, stiff*, colloids with stiff chains attached with an exit angle constraint and harmonic spring.

For each colloid type, we consider 25 different surface (q_c) and polyelectrolyte (q_p) charge combinations in the range $0.5e$ to $-2.5e$ and $-0.5e$ to $-2.5e$, respectively. The largest surface charge densities $\sim$0.6e/nm^2 examined here are well within reach of biological membranes and nanoparticles. Similarly, the strongest polyelectrolyte charges used here are within experimental bounds; consider our highest line charge density of $2.5e$/nm to that of dsDNA ($\sim 6e$/nm). Note that though some charge combinations do not yield neutral colloids, i.e., $n_c q_c \neq N n_p q_p$, the Debye−Hückel formulation used here implies overall (solution plus colloid) electroneutrality. Also, we choose to vary charges by modulating the charge magnitude while keeping the number of charged beads fixed instead of varying the number of beads and keeping the charge/bead fixed because this approach results in uniform charge distributions along the surface and chain length.

The PMFs and their energy and entropy contributions are computed at distance increments of 1 nm in the range $d = 21-35$ nm for each colloid type and charge combination. To achieve better sampling, we performed four independent simulation runs for each colloid type, charge combination, and separation distance. Small deviations between the results computed from the four simulation copies suggested that the sampling was ergodic. The simulations were performed on 3.2 GHz Intel EM64T processors and demanded about 30 000 h of total CPU time. All other parameters such as colloid size, chain length, force field, temperature, and salt concentration are fixed throughout the study.

3. Results

3.1. Chain Configurations. To examine the effect of chain stiffness and attachment mode on the chain configuration in *isolated* colloids, we compute two quantities. First, we compute the fraction of chains adsorbed at the colloid surface, f_{ads}, where a chain is considered "adsorbed" when one or more of its three terminal beads lie within 1 nm of the surface. Second, we compute the average extension of chains, d_{ext}, defined as the distance from the surface of the colloid enclosing 95% of the chain beads, as given by

$$\frac{\int_R^{d_{ext}+R} 4\pi r^2 \rho(r) \, dr}{\int_R^{\infty} 4\pi r^2 \rho(r) \, dr} = 0.95 \quad (13)$$

where $\rho(r)$ is the average chain bead density at a distance r from the center of the colloid computed from the MC simulation. Figure 2 shows f_{ads} as a function of surface and polyelectrolyte charges for the four types of colloids. The plots for d_{ext} are included in Supporting Information Figure S1 and provide essentially the same trends as the plots for f_{ads}. The results are presented as contour plots using the MATLAB routine *contourf*.

All four colloids exhibit qualitatively similar trends. The chains extend away from the surface when the surface and polyelectrolyte chains are weakly charged, as noted from the small f_{ads} values. As the two colloids become more charged, the chains collapse at the surface due to their increased attraction with the surface, whose magnitude scales roughly as $|q_c q_p|$. Indeed, the contour lines seem to follow curves of the type $|q_c q_p| \simeq$ constant. By $(q_c, q_p) = (2.5e, -2.5e)$, almost 80−90% of the chains are collapsed at their surface. These trends can also be gleaned from representative snapshots of the colloids at varying charge values provided in Supporting Information Figure S2.

While there is little difference between colloids with free or constrained chains when they are flexible (Figure 2a, c), strong differences appear for stiff chains. For colloids with freely attached chains, increasing the chain stiffness causes the chains to collapse less and extend more (Figure 2a, b). Also, the range of q_c and q_p values over which the chains remain extended becomes larger for the stiff chains, i.e., the extended to collapse transition of the chains is "delayed" in the charge space. This

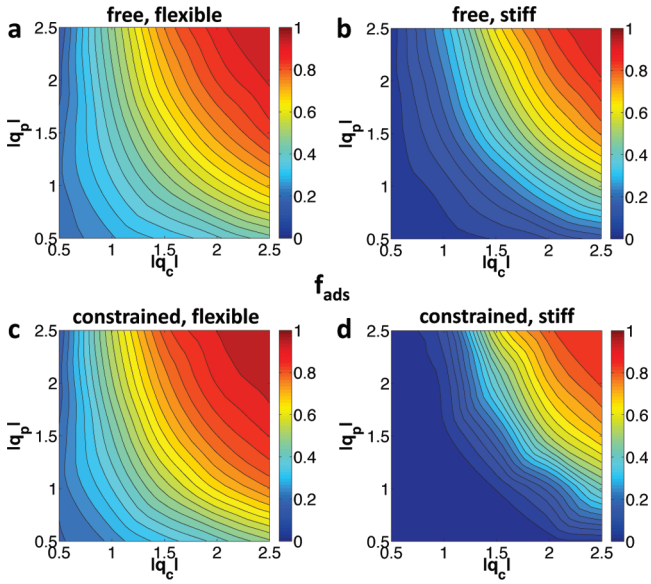

Figure 2. Fraction of surface-adsorbed chains (f_{ads}) as a function of surface and polyelectrolyte charge in isolated colloids with (a) free, flexible; (b) free, stiff; (c) constrained, flexible; and (d) constrained, stiff chains.

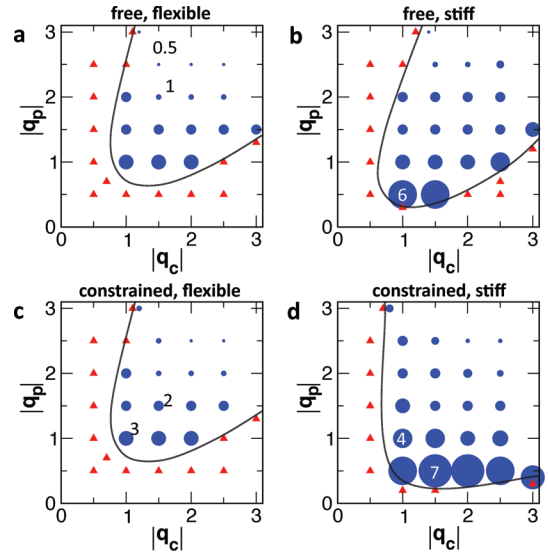

Figure 3. Extent and range of the attractive regime in the q_c-q_p space for colloids with (a) free, flexible; (b) free, stiff; (c) constrained, flexible; and (d) constrained, stiff chains. Blue circles and red triangles represent attractive and purely repulsive PMFs at the specified surface and polyelectrolyte charges, respectively. The black dashed curves help demarcate the attractive regime from the repulsive regime. The green dashed line represents overall neutral colloids. The diameter of the blue circles is directly proportional to the range of attraction. The numbers on some circles or next to some circles specify the attraction range in nanometers for those charge combinations.

transition is gradual and not sharp like a first-order phase transition; however, one can approximately define the location of the transition by the condition $f_{ads} = 0.5$. The effect of chain stiffness is more stark in colloids with constrained chains. Here, the stiff chains remain extended for a larger range of q_c and q_p values (Figure 2c,d). In fact, there is not a single chain that remains collapsed at $(q_c, q_p) = (1e, -1e)$, compared to 10% in the case of free, stiff chains and >30% in the case of free or constrained flexible chains. In fact, the chains are so extended here that d_{ext} approaches 7 nm, the length of straight chains (see Figure S1). In contrast, d_{max} only approaches 4 nm in flexible-chain colloids. Evidently, the energetic penalty for the chains to bend backward and adsorb at their own surface is too large. The chain extended to collapse transition is also more abrupt in constrained, stiff chains compared to freely attached chains.

We have also examined chain configurations for the two-colloid system when the two colloids are in close proximity ($d = 22$). Supporting Information Figures S3−S5 show the contour plots of chain monomer densities for colloids with free, flexible; free, stiff; and constrained, stiff chains. The plots for colloids with constrained, flexible chains are not shown due to their close similarity to those for colloids with free, flexible chains. The contour plots are constructed by computing the local monomer density along planar slices of thickness 1 nm passing through the centers of two colloids and averaging this density over an ensemble of slices oriented at angles in the $[0, \pi]$ range.[5]

The plots echo the differences in the chain extended-to-collapsed transitions in the four colloid types discussed above, i.e., the transition becomes increasingly abrupt and delayed in the q_c-q_p charge space in the following order: flexible chains (both free and constrained), stiff, freely attached chains, and stiff, constrained chains. More importantly, the plots show accumulation of chains in the gap between colloids, which is partly attributed to the overlap of chains from two surfaces and partly to the favorable electrostatic potential due to the presence of the two charged surfaces. While the chain densities outside the gap, close to the colloid surface, generally increase monotonically with increasing q_c and q_p (due to chains collapsing onto the surface), the chain densities within the gap exhibit a more complex behavior. For a fixed surface charge q_c, the gap densities first increase with increasing q_p, exhibit a maximum, and then decrease with further increase in q_p. The initial increase in chain density arises from increased attraction between chains and surface, but as q_p increases further, the chain/chain repulsion, whose magnitude scales as q_p^2, begins to dominate and the chain density decreases to minimize this repulsion. We also note differences in the spatial extent of chain density along the radial direction in the gap between the two particles. This extent, indicative of the number of polymer-bridging interactions, increases in the following order: free, flexible → free, stiff → constrained, stiff. Clearly, the stiffer chains remain more extended and have a farther reach, thus allowing chains further away from the two-colloid axis to still mediate polymer-bridging interactions.

3.2. Effective Interactions between Colloids. To examine the effect of chain stiffness and attachment mode on the effective interactions between the colloidal particles, we compute the distance-dependent PMF, $\mathcal{M}(d)$, of two particles at different q_c-q_p combinations. The computed PMFs are used to map out the attractive-force regime within q_c-q_p space. A PMF is characterized as attractive if $\mathcal{M}(d) < 0$ *anywhere* within the $2R < d < \infty$ range, and repulsive if $\mathcal{M}(d) > 0$ for the entire range.[5]

Figure 3 shows the extent of the attractive regime within the q_c-q_p space for the four colloid types examined, where the boundary of the attractive regime is represented by the dashed, hyperbola-shaped curve. The blue circles, which represent charge combinations at which the PMF is attractive, occupy the region inside the hyberbola, while the red triangles, which represent the repulsive region, occupy the region outside. The size of these circles is directly proportional to the range of attraction R_a defined as the distance between two colloid surfaces at which they exhibit the strongest attraction, i.e., $R_a = d_m - 2R$, where d_m is the center-to-center distance between two colloids at the PMF minimum. We note that the attractive regimes for all colloids orient themselves symmetrically in the

q_c-q_c space with their major axis aligning roughly in the direction of the dashed red line corresponding to neutral colloids, where $n_c q_c = N n_p q_p$ (we refer to this line henceforth as "neutral-colloid line"). Additionally, none of the hyperbola boundaries intersect the origin, implying that all four colloids are repulsive in the small q_c and q_p (neutral) limit. For colloids with freely attached chains, the effect of increased chain stiffness on the extent of the attractive regime is only marginal (Figure 3a, b), as characterized by a slight extension (shift) of the attractive regime toward weak charges. The increase in chain stiffness leads to a more dramatic effect when the chains are attached in a constrained manner (Figure 3c,d). Specifically, the attractive regime becomes significantly broader within the charge space, and, as in the case of freely attached chains, the attractive regime extends slightly toward weak charges. Also, the mode of chain attachment has little impact on the extent of the attractive regime when the chains are flexible, as explained earlier in terms of chain configurations.

Turning to the extent of attraction, we note that the attraction is long-ranged when both q_c and q_p are small, i.e., when the chains are highly extended. As the system become more strongly charged along the neutral-colloid line, the attraction becomes more short-ranged, consistent with the collapse of chains at their own surface (Figure 2). Comparing R_a values of the four colloid types, we note that R_a generally increases with chain stiffness for both free (Figure 3b) and constrained chains (Figure 3d). In fact, R_a approaches 7 nm, the length of fully stretched chains, for colloids with constrained, stiff chains at small q_c and q_p (Figure 3d). Also, as expected, very small differences are noted between the R_a values of flexible and stiff chains when the chains are freely attached (Figure 3a,c). We also note the existence of a strong correlation between R_a and chain extensions, which suggests that the attraction between colloids may be mediated by polymer-bridging interactions.

Finally, we examine the strength of attraction, $\Delta\mathcal{A}$, characterized by the value of the PMF at a separation distance of $d = 22$ nm. We choose this particular distance as a reference point for comparing $\Delta\mathcal{A}$ across different charges, chain stiffnesses, and attachment modes, as many PMFs exhibit a minimum at this distance. Figure 4 shows the contour plot of $\Delta\mathcal{A}$ in the q_c-q_p space for the four colloids. Note that the $\Delta\mathcal{A} = 0$ contour line may be slightly different from the hyperbolic boundary plotted in Figure 3, as the former only consider the value of the PMF at $d = 22$ nm while the latter searches along the entire range $d > 20$ nm to assess if the PMF is attractive or repulsive. All four contour plots show that the attraction is the strongest along the neutral colloids line. As the charges deviate from this line, the attraction becomes weaker until it converts to repulsion for strongly differing $|q_c|$ and $|q_p|$. The attraction also becomes stronger with increasing charge magnitude along the neutral colloids line for all four colloids. The contour profiles also show strong dependence on the chain stiffness and their attachment mode. Most notably, the colloids with constrained, stiff chains (Figure 4d) exhibit a signficantly stronger attraction than those with flexible chains (Figure 4c). The attraction free energy becomes as large as -35 kcal/mol for $(q_c, q_p) = (2.5e, -2.5e)$ for stiff chains, compared to -12 kcal/mol for flexible ones with the same set of charges. The trend is very different for colloids with freely attached chains. Here, the attraction is weaker in stiff chains (Figure 4b) compared to flexible ones (Figure 4a). For example, the attraction energy is roughly -7 kcal/mol for stiff chain colloids at $(2.5e, -2.5e)$ compared to -12 kcal/mol for flexible ones at the same charges.

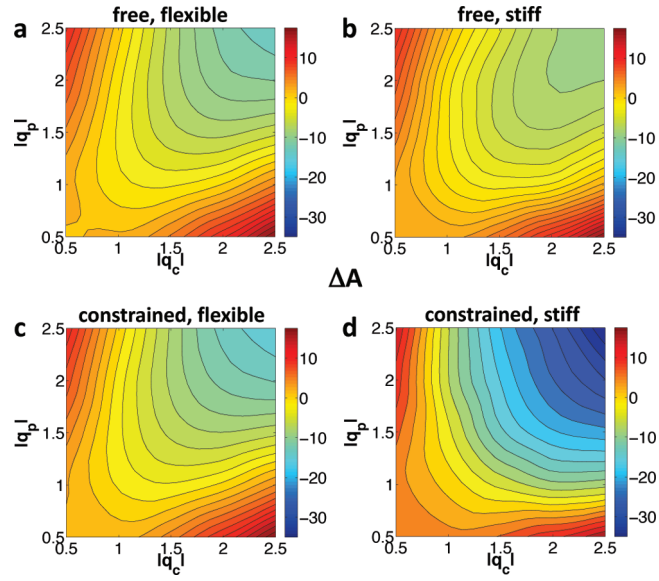

Figure 4. Total free energy change $\Delta\mathcal{A}$ associated with bringing two colloidal particles from infinity to $d = 22$ nm as a function of surface and polyelectrolyte charges. The four plots correspond to colloids with (a) free, flexible; (b) free, stiff; (c) constrained, flexible; and (d) constrained, stiff chains.

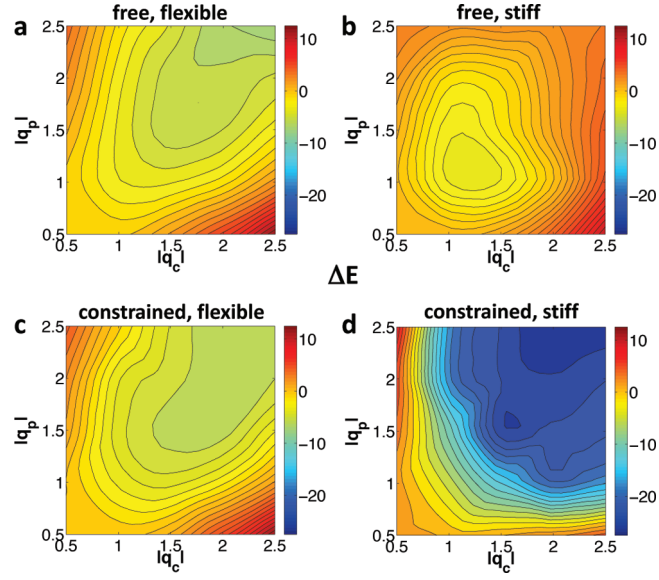

Figure 5. Total energy change $\Delta\mathcal{U}$ associated with bringing two colloidal particles from infinity to $d = 22$ nm as a function of surface and polyelectrolyte charges. The four plots correspond to colloids with (a) free, flexible; (b) free, stiff; (c) constrained, flexible; and (d) constrained, stiff chains.

To understand the above differences in the attraction between colloids with flexible and stiff chains attached in a free or constrained manner, we have decomposed the PMF into its energetic and entropic contributions. Figure 5 shows a contour plot of the total energy of two colloids separated by a distance $d = 22$ nm *relative* to that of two isolated colloids ($\Delta\mathcal{U}$). Figure 6 shows the corresponding difference in the total entropy of the two systems ($\Delta\mathcal{S}$). We first review the "classical" energy and contour plots obtained for colloids with free, flexible chains (Figures 5a and 6a), introduced in our earlier study.[5] These plots will serve as reference points for all subsequent discussions on the effects of chain stiffness and attachment.

3.3. Energetic and Entropic Contributions in Colloids with Flexible Chains. The energy contours (Figure 5a) show a parabolic region of favorable energies that nearly extends to

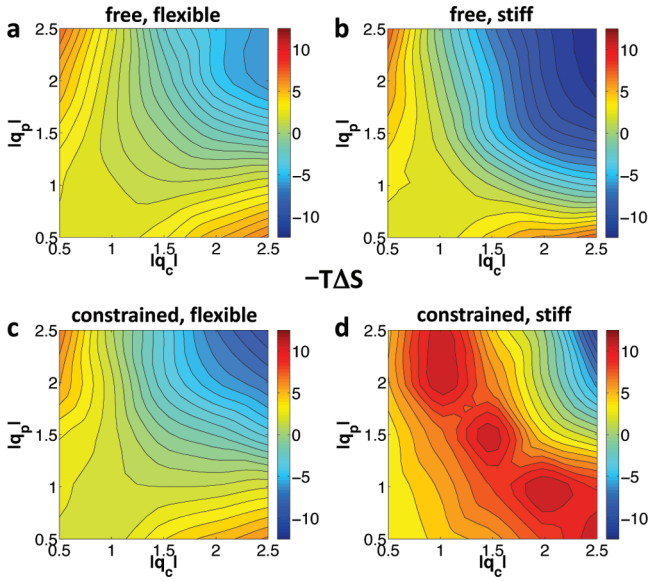

Figure 6. Total entropy change $-T\Delta\mathcal{S}$ associated with bringing two colloidal particles from infinity to $d = 22$ nm as a function of surface and polyelectrolyte charges. The four plots correspond to colloids with (a) free, flexible; (b) free, stiff; (c) constrained, flexible; and (d) constrained, stiff chains.

zero charge. The most favorable energies occur along the neutral-colloid line, and they become less favorable with deviations from this line and more favorable with increasing charge along the line. The specific shape of the attractive regime can be explained in terms of the three dominant interactions: electrostatic repulsion between surfaces, electrostatic repulsion between chains, and electrostatic attraction between the chains and surfaces. The repulsive terms dominate the attractive terms when q_c and q_p are very different in magnitude. As the two become comparable and the colloids become net neutral, the attractive terms begin to dominate, leading to favorable energies. The energies become more favorable with increasing charge along the neutral-colloid line because the chain/surface attractive energies generally rise faster than $|q_c q_p|$ while the surface/surface repulsion rises as q_p^2 and the chain/chain repulsion rises slower than q_p^2.[5] Further decomposition of the chain/surface interactions shows that the favorable energies result from polymer-bridging interactions, where chains from one colloid adsorb onto the surface of the second colloid, rather than from remote interactions between one surface and the "cloud" of polyelectrolyte chains surrounding the other surface.[5]

The entropy landscape (Figure 6a) is very different from the energy landscape. The entropy loss is moderate when both q_c and q_p are small. This is primarily dictated by the overlap of chains from the two colloids, which reduces their configurational freedom. The entropy loss due to chain overlap becomes substantial when $|q_c| \ll |q_p|$ due to increased extension of chains (see Figures 2a, S1a). The increased repulsion among chains in this charge regime, which increases the effective excluded volume of the chain beads, further magnifies the loss in chain entropy. The entropy loss is also substantial when $|q_c| \gg |q_p|$. Here, it is the accumulation of chains in the gap between the colloids that leads to their reduced entropic freedom. Finally, the entropy change becomes favorable when both q_c and q_p are large, and $T\Delta\mathcal{S}$ can be as large as 5−6 kcal/mol for strong charges (Figure 6a). This gain in entropy is attributed to polymer-bridging interactions, where the chains gain freedom when the two colloids come in close proximity, as it allows collapsed chains to desorb from their own surface and adsorb at the apposing colloids' surface.

The energy and entropy landscapes combine to produce the PMF landscape of Figure 4a. The weak repulsion observed at small q_c and q_p occurs due to weakly favorable energies being dominated by more unfavorable entropies. As q_c (or q_p) increases along the neutral-colloid line, both the entropy and energy become more favorable, leading to an increased attraction. When $|q_c|$ and $|q_p|$ are very different, the unfavorable energies and chain entropies result in a strong repulsion. The above energy and entropy landscape features also hold for colloids with constrained, flexible chains, given that the chains in the two colloid types exhibit very similar conformations (Figure 2). However, this classical picture does not hold completely true for colloids with stiff chains, both free and constrained, and we discuss below how deviations from this lead to the marked differences in their PMF contours in Figure 4b,d.

3.4. Effect of Chain Stiffness in Colloids with Freely Attached Chains. The energy landscape of colloids with flexible chains (Figure 5a) and stiff chains (Figure 5b) share several common features such as the unfavorable energies that result when q_c and q_p differ strongly in magnitude and the favorable energies that result when the two charges become more comparable. However, there is one striking difference between the two landscapes. While the attraction energy for flexible-chain colloids becomes more favorable in a monotonic fashion with increasing charge along the neutral-colloid line, the energy of the stiff-chain colloids exhibits a nonmonotonic dependence. In particular, there exists an "island" of strong attraction at $(q_c,q_p) \approx (1e, -1e)$, and the energies become more unfavorable beyond it.

To determine the source of unfavorable energies in stiff-chain colloids at large q_c and q_p values, we break down $\Delta\mathcal{U}$ for flexible and stiff-chain colloids into their individual contributions for two sets of charges: $(1e, -1e)$, where $\Delta\mathcal{U}$ is favorable for both colloid types, and $(2e, -2e)$, where the $\Delta\mathcal{U}$ is favorable for flexible-chain colloids and unfavorable for the stiff-chain colloids. At $(1e, -1e)$, all energy components of flexible-chain colloids are roughly similar to those of stiff-chain colloids. This is no longer true for $(2e, -2e)$, where chain bending energy ΔE_b increases from 0 to 1.5 kcal/mol, the polymer/polymer repulsion energy ΔE_{pp} increases from 17.8 to 19.1 kcal/mol, and the electrostatic attraction between the chain and surface ΔE_{cp} increases from −40.5 to −35.9 kcal/mol as the chains go from flexible to stiff. Hence, the larger $\Delta\mathcal{U}$ in stiff-chain colloids (1.9 kcal/mol) in comparison to flexible-chain colloids (−5.3 kcal/mol) is a result of unfavorable changes in chain bending, chain/chain interactions, and chain/surface interactions. The first effect arises from the larger bending constant k_θ in stiff chains that leads to larger energy penalties when the chains contort themselves to accommodate the approaching colloid. The second effect arises from the reduced ability of stiff chains to adopt favorable configurations for mitigating repulsion among chains as the colloids are brought closer. The last effect arises from the stronger adsorption of stiff chains compared to flexible chains: While the stiff chains mediate more polymer-bridging interactions than flexible chains, as noted by their stronger "intercolloid" attraction ΔE_{cp2} (−5.3 kcal/mol), they also sacrifice a greater amount of favorable energy resulting from adsorption of chains at their own surface when the chains desorb, as noted by the less favorable "intracolloid" attraction ΔE_{cp1} (+9.8 kcal/mol). Supporting Information Table S1 tabulates the magnitude of all energy contributions for the two types of colloids at the two charge combinations.

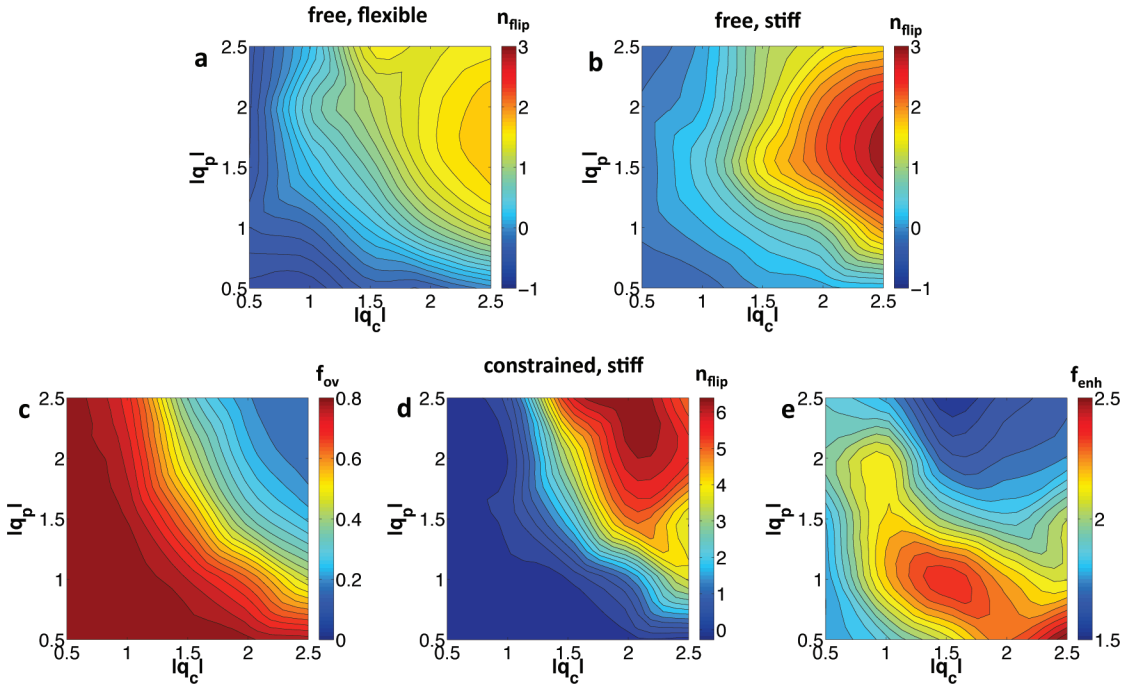

Figure 7. (Top) Number of chains flipping from surface-adsorbed to bridging conformations (n_{flip}) when the colloids with (a) free, flexible and (b) free, stiff chains are brought from infinity to a distance $d = 22$ nm for colloids. (Bottom) (c) Fraction of chains overlapping (f_{ov}), (d) n_{flip}, and (e) enhancement in chain density in the gap (f_{enh}) when colloids with constrained, stiff chains are brought from infinity to $d = 22$ nm.

Though the entropy landscape of stiff-chain colloids (Figure 6b) exhibits a similarity with that of flexible chain-colloids (Figure 6a), the entropy change is notably larger in the former, especially at large q_c and q_p values. For example, at (2.5e, −2.5e), $T\Delta S = 12$ kcal/mol in stiff-chain colloids, almost twice that of flexible-chain colloids.

To explain this difference, we have computed three quantites (at $d = 22$ nm) that we believe contribute the most to entropic changes when the two particles are brought near each other:[5] the fraction of chains overlapping in the gap between colloids (f_{ov}); the enhancement in the chain density within this gap (f_{enh}), calculated as the ratio of the chain density in the gap between colloids and the chain density outside the gap equivalent to the chain density in isolated colloids; and the number of chains that desorb from their own surface and adsorb on the apposing colloid's surface to mediate polymer-bridging interactions (n_{flip}). The first two effects lead to entropy loss, and the third effect is entropically favorable.[5] The results are plotted in Figure 7 as contour plots in the q_c−q_p space. The stronger entropy gain in stiff-chain colloids may be attributed to the larger number of flipped chains n_{flip} in the stiff-chain colloids (Figure 7b) compared to those in flexible-chain colloids (Figure 7a). However, the difference in n_{flip} seems to be too small to yield the large entropy differences of 6 kcal/mol observed between the two colloid types. It should, however, be noted that n_{flip} does not take into account the much stronger adsorption of stiff chains at their own surface (and hence much less entropic freedom) compared to the flexible chains. Hence, the entropic gain per chain is much larger for stiff chains compared to the flexible chains. The slightly smaller degree of chain overlap and density enhancement in stiff chains at large q_c and q_p likely also contribute a little to the larger entropy gain observed in stiff-chain systems (see Supporting Information Figure S6).

In summary, the unfavorable energy associated with chains desorbing from their own surface to mediate polymer bridging is the main contributor to the weaker attraction observed in colloids with stiff, freely attached chains, despite the entropy gained from such bridging interactions.

3.5. Effect of Chain Stiffness in Colloids with Constrained Chains. Both the flexible and stiff-chain colloids exhibit favorable energies along the neutral-colloid line, which become increasingly unfavorable as the charges deviate from this line. However, there exist two striking differences between the two colloids types. First, the $\Delta\mathscr{U}$ values for stiff-chain colloids are considerably more favorable than those of flexible-chain colloids. For instance, $\Delta\mathscr{U}$ can reach values as large as −25 kcal/mol in stiff-chain colloids at large q_c and q_p. Second, the energy contours of stiff-chain colloids are significantly broader in the charge space than those of the flexible-chain colloids.

To explain the highly favorable energies of the constrained, stiff-chain colloids, we have computed the energy contributions of all colloids types at two sets of charges along the neutral-colloid line, (1e, −1e) and (2e, −2e) (see Supporting Information Table S1). We find that the main contribution to the highly favorable energy of −24 kcal/mol of stiff-chain colloids at (2e, −2e) arises from the significant loss in chain-bending energy ($\Delta E_b \approx -32$ kcal/mol). In fact, the net change in the electrostatic energy is large and positive, but the highly favorable ΔE_b more than compensates the unfavorable electrostatic energy. Such a favorable contribution from chain bending is missing in the remaining three colloid types. The loss in bending energy may be understood by inspecting chain configurations of free, stiff and constrained, stiff chains at (2e, −2e) and $d = 22$ nm (Figure 8). Most chains in both colloid types (other than those mediating polymer-bridging interactions) are strongly adsorbed at their own surface. However, there is a key difference in how the two chain types adsorb. In freely attached chains, all chain beads lie close to the surface (Figure 8a). Since these chains do not incur any bending energy penalty in adsorbing at the surface, the change in bending energy associated with them desorbing and mediating polymer-bridging interactions is minimal. In contrast, the stiff, constrained chains do not hug the surface as closely but form loops partially elevated from the surface before their terminal beads adsorb back onto the surface (Figure 8b). Here, the stiff, harmonic constraint on the angle subtended by the first two beads and the colloid (Figure 1c) makes the chains emerge

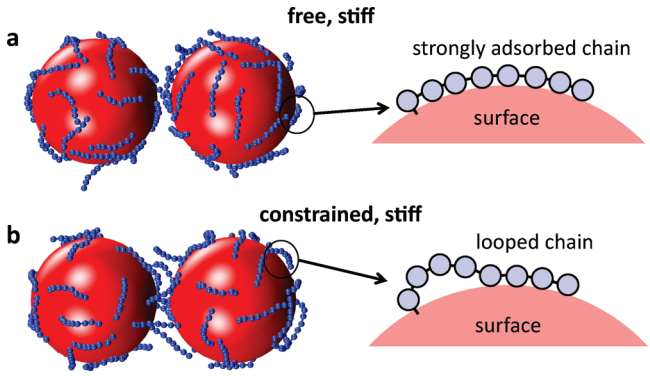

Figure 8. Snapshots of colloids with (a) free, stiff and (b) constrained, stiff chains at $(q_c, q_p) = (2e, -2e)$ at $d = 22$ nm showing surface-adsorbed and polymer-bridging conformations of the chains. Also shown on the right-hand side are schematics of the chains highlighting differences in how the chains are adsorbed at the surface for the two types of colloids.

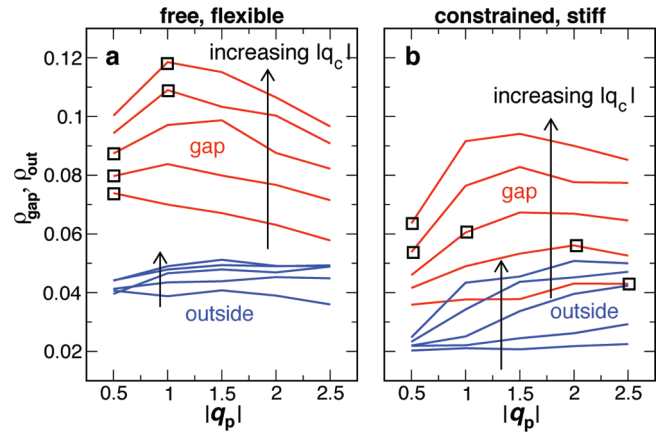

Figure 9. Chain density in the gap between two colloids particles separated at $d = 22$ nm (ρ_{gap}; red lines) and outside the gap (ρ_{out}; blue lines). The densities are plotted as a function of polyelectrolyte charge at fixed surface charge for colloids with (a) free, flexible and (b) constrained, stiff chains. The density curves shift upward with increasing q_c.

almost perpendicular to the surface, and the first few bonds in the chain need to bend to form the loop and allow adsorption of the terminal beads at the colloid surface, resulting in a large bending energy penalty. When another colloid is brought nearby, the looped chains desorb from their own surface and straighten out to mediate polymer-briding interactions, which releases a large amount of stored bending energy, thus explaining the highly negative ΔE_b.

A similar argument can explain why flexible, constrained chains do not exhibit such a favorable bending energy change. In this case, the chains do not adsorb as strongly as the stiff chains. In addition, the bending constant is weak and the chains incur little bending energy penalty for adsorbing at their own surface leading to small ΔE_b. The above chain bending argument also explains why colloids with stiff, constrained chains exhibit such a broad region of favorable energies compared to other three colloid types (see Supporting Information Table S2 and the related discussion).

The entropy contours of stiff-chain colloids clearly do not exhibit the traditional landscape of the flexible-chain colloids. The most obvious difference is that the unfavorable entropies in these colloids are not restricted to large q_c−small q_p and small q_c−large q_p corners of the charge space (Figure 6a), as in flexible-chain colloids, but occur along a concave "arc" joining the two corners (Figure 6d). Other features such as the most favorable entropies occurring at large q_c and q_p remain unchanged for stiff-chain colloids, though these entropies are much larger than those observed in flexible-chain colloids. To understand the origin of this arc of unfavorable entropies, we analyze the fraction of chain overlap (f_{ov}), the chain density enhancement (f_{enh}), and the number of flipped chains (n_{flip}) in colloids with constrained, stiff chains (Figure 8c−e). We note that the arc trajectory in the q_c−q_p space coincides with the onset of the extended-to-collapse transition of the chains, i.e., the set of surface and polyelectrolyte charge values at which the chains begin to strongly collapse at the surface (see also Figure 2d). Since the chains remain extended here, f_{ov} is large (Figure 8c) and n_{flip} is small (Figure 8d). Interestingly, strong density enhancement f_{enh} values also follow the arc (Figure 8e). Clearly, this arc of large f_{enh} values combined with large f_{ov} values and small n_{flip} values are responsible for the arc of unfavorable entropies across the charge space observed in colloids with constrained, stiff chains.

What is the origin of the large f_{enh} arc across the charge space? We recall that f_{enh} is given by the ratio of the chain density in the gap between colloids ρ_{gap} to that outside ρ_{out}. Figure 9 compares the two densities, computed at $d = 22$ nm, for colloids with constrained, stiff and free, flexible chains. For stiff, constrained chains (Figure 9b), ρ_{out} increases monotonically with q_p for all q_c. The increase is gradual for small q_p, as the chains prefer to remain extended, then sharp at the onset of the extended-to-collapse transition, and then gradual again, as most of the chains have collapsed. In contrast, the gap density ρ_{gap} increases sharply with q_p for small q_p, due to increased polymer bridging, and then decreases gradually as q_p becomes large and the chain/chain repulsions dominate. Both trends (in ρ_{open} and ρ_{gap}) become more pronounced for large q_c, with ρ_{open} exhibiting the sharper change of the two. At the same time, the location of the extended-collapsed transition also shifts toward smaller q_p values. The combined effect is that q_p values at which f_{enh} exhibits the maximum value (squares in Figure 9b) shift to lower values with increasing q_c, thus following a path in q_c−q_p space that resembles the arc seen in Figure 6d. In contrast, the free, flexible chains (Figure 9a) are already half-collapsed at the smallest q_c and q_p values considered here ($0.5e$, $-0.5e$). Hence, the chains undergo a much milder extended-collapsed transition compared to constrained, stiff chains. This results in a marginal rise in ρ_{out} for $q_c > 0.5e$ and a slight decrease for $q_c = 0.5e$ with increasing q_p. At the same time, ρ_{gap} exhibits a sharp increase followed by a steady decline with increasing q_p. These trends lead to f_{enh} exhibiting maximum values at low q_p values (squares in Figure 9a) and explain why these colloids do *not* exhibit the arc of high f_{enh} seen in constrained, stiff colloids. The same argument explains why the stiff, free colloids also exhibit f_{enh} maximas at low q_p values only.

In summary, the primary contributor to the extremely strong attraction observed in colloids with stiff, constrained chains, especially at strong surface and polyelectrolyte charges, is the release in bending energy of chains as they desorb from their own surfaces to mediate polymer-bridging interactions. The favorable entropies arising from this mechanism further contribute to the attraction.

4. Discussion

The main finding of this study is that the stiffness of polyelectrolyte chains could have completely different effects on the interactions between polyelectrolyte-grafted colloids

depending on how the chains are attached to the surface. When the chains are freely attached, an increase in chain stiffness leads to reduced attraction between the colloids. We show that this reduction is mainly attributed to the larger energy sacrifice made by stiffer chains in desorbing from their own surface to mediate polymer-bridging interactions with the apposing colloid. This increased desorption penalty for stiff chains along with their increased chain/chain repulsion and bending energies outweighs their larger entropy gain from polymer bridging to reduce the net attraction between the colloids. When the chains are attached with an angle constraint, the effect of chain stiffness is drastically different. Here, the stiff-chain colloids exhibit a much stronger and broader attractive regime in the charge space compared to flexible-chain colloids. The main contributor to this strong attraction is the release of large amounts of bending energy stored in the stiffer chains when the chains desorb from their own surface to mediate polymer-bridging interactions with the apposing colloid. This effect along with the more favorable polymer-bridging entropy in stiff chains explains the observed strong and broad attraction. The underlying cause for these differences in interactions is the extended-to-collapse transition, which is very sensitive to the attachment mode in the case of stiff chains.

A particularly surprising result is the significant increase in attraction observed with the stiffness of the chains when they are surface-attached in a constrained manner, which goes against the common notion that increased stiffness should lead to stronger steric repulsion between chains.[1] However, it should be noted here that our colloids are grafted at a low density, with short chains, where steric repulsion effects are expected to be weak. We also observe that polymer bridging and not charge correlations are responsible for the attraction observed in our colloids. This may be deduced from the strong correlation observed between the range of attraction and chain extension (Figure 3), the favorable entropies observed with strong charges typical of polymer bridging (Figure 6), and the more negative polymer-bridging energies compared to the total free energy of attraction.[5] The observed attraction is therefore different from the short-range attraction observed by Turesson et al.,[17] who examined two charged surfaces confining *free-floating* semirigid polyelectrolyte chains. In that study, the rigid chains lay flat at the two surfaces and oriented themselves almost parallel to each other. No bridging of chains was observed across the surfaces, and the attraction was attributed to charge correlations between the two layers of adsorbed chains. Our polyelectrolyte chains do *not* exhibit this behavior as a large fraction of the chains between the intercolloid gap are involved in bridging interactions.

It is also instructive to compare the behavior of our colloids to their neutral counterparts, uncharged colloids grafted with neutral polymers. In general, neutral polymer-grafted colloids at sufficiently high grafting density or long chains are always repulsive in good solvents due to the strong steric repulsion between the chains.[1,31,32] However, for sparse grafting and short chains, the van der Waals forces between the colloids can sometimes become strong enough to overcome the weak steric repulsion.[1] An attraction can also be introduced by dispersing macromolecules in the solution that introduce additional effects like depletion interactions.[31,33,34] However, *our* polyelectrolyte-grafted colloids when made neutral by setting q_c and q_p to zero always exhibit a repulsion. This is because the van der Waals attractions between the colloids are very weak and cannot overcome the steric repulsion between the polymer chains due to their overlap. As we show in this study, introducing charges to the grafted polymers and colloid surfaces causes the colloids to exhibit both repulsion and attraction, depending on the relative magnitude of the two charges. Compared to neutral colloids, the repulsion is stronger in charged colloids as it arises from both steric and electrostatic effects, especially when q_c and q_p have very different magnitudes. The attraction is also much stronger than k_BT as it is caused by electrostatic interactions operating at short length scales (polymer bridging). Also, the attraction occurs at separation distances comparable to the extent of the polymer chains that allows bridging of polymers without significant steric interactions. Indeed, we expect that as the grafting density of our chains is increased or when the chains are made longer, the steric effects will come into play and the attraction will be mitigated.

Our findings have several important implications. First, the dramatic differences observed here in the interactions for chains attached freely or in a constrained manner when the chains are relatively stiff underscore the importance of the mode of attachment of polyelectrolytes to the surfaces. This implies that computational models used for studying the interactions and self-assembly of polyelectrolyte-grafted colloids need to correctly account for chain attachment and local interactions with the surface, especially when the chains are stiff, as defined by a sharp extended-to-collapsed transition. Similarly, the synthesis of polyelectrolyte-grafted colloids should also not ignore the effects of surface attachment. Second, though the importance of the mode of attachment introduces an additional layer of complexity to the problem of interactions between colloids, it also offers an additional control parameter for tuning the interactions between colloids for applications such as bottom-up self-assembly of nanostructured materials from colloidal particles of various shapes and sizes grafted with polymers[23,24] and biomolecules like DNA,[35,36] especially when other system parameters have limited freedom.

Finally, it would be interesting to experimentally test our computational predictions on the differences between colloids with constrained and freely grafted polyelectrolyte using current approaches for attaching polymer chains to surfaces, e.g., physisorbtion and covalent grafting (both grafting-from and grafting-to approaches). Indeed, researchers have begun to examine interactions between colloids in the context of DNA-grafted colloids using powerful single-molecule experimental techniques like optical tweezers.[36] We should, however, point out that our model makes several approximation, and one should only expect qualitative agreement between theory and experiments. One approximation is the use of the Debye−Hückel potential to treat screened electrostatic interactions. It is well-known that this approximation cannot treat charge correlation effects, which could arise in systems with strongly charged surfaces and multivalent ions, and interactions in nanometer-sized confinements, due to neglect of the size of ions. Most colloids employed in this study correspond to the weak-to-moderate electrostatic coupling regime, as determined by computing the coupling parameter ($\Xi \approx 1.8$ for the strongest charges examined[37]) and the ratio of electrostatic to thermal energies for a surface and polyelectrolyte charge separated by the distance of closest approach. We therefore expect this approximation to do a fair job in treating salt-screened electrostatic interactions. Other approximations include coarse-graining of the polymers and the colloid, which could mask finer effects arising from the surface corrugation, atomic-scale structure of the polyelectrolytes, and distribution of charges. We also neglect solvation effects and hydration of the chains and surface and assume a neutral (theta-like) solvent.

5. Conclusions

We have elucidated the effect of polyelectrolyte chain stiffness and their mode of attachment on the effective interaction (potential of mean force) between polyelectrolyte-grafted colloids over a broad range of polyelectrolyte and surface charges using Monte Carlo simulations. Our system represents nanoparticles grafted with short polyelectrolytes at a low grafting density dispersed at low concentration within an inert solvent. Two different chain stiffnesses and two different modes of chain attachment to the surface have been examined. In one attachment mode, there exists a strong constraint on the "exit" angle at which the chains emerge from the colloid surface, and in the other mode, no such constraint exists and the chains are free to exit at any angle from the surface.

Both chain stiffness and attachment mode are found to have a dramatic impact on the interactions between colloids. When the chains are attached freely to the surface, an increase in the chain stiffness leads to weaker effective attraction between the particles without major changes to the extent and shape of the attractive-force regime within the surface-polyelectrolyte charge space. The effect of chain stiffness is very different when the chains are attached in a constrained manner. Here, the increase in stiffness considerably strengthens the attraction between the particles and broadens the attractive regime within the charge space. We have uncovered the detailed mechanisms responsible for these differences in terms of energetic and entropic contributions. Specifically, we have shown that the reduced attraction in freely attached chains occurs due to stronger collapse of stiff chains at their own surface compared to that of flexible chains. This results in a considerably larger energetic penalty than the entropic gain for mediating polymer-bridging interactions in the case of stiff chains. We have also shown that the stronger attraction and broadening of the attractive regime in the case of constrained chains arise due to a novel mechanism involving release of stored bending energy in the case of stiff chains collapsed at the surface. Our analyses also show the different collapse-to-extend transition of chains as being the underlying cause of the dramatic differences.

Apart from uncovering and explaining new, interesting effects of chain stiffness and their attachment, our study has several other implications. First, how chains are grafted onto the surface cannot be ignored in the computational modeling of such systems and their experimental synthesis, and second, chain attachment configuration could be used as an additional control parameter to modulate interactions between charged colloidal particles.

Acknowledgment. Computer time on the Granite cluster of the bioengineering department at U. C. San Diego is acknowledged.

Supporting Information Available: Tables showing individual contributions to the total interaction energy of colloids and figures showing chain extension contour plots, representative chain configurations, monomer density contour plots, and f_{enh} and n_{flip} contour plots. This material is available free of charge via the Internet at http://pubs.acs.org.

References and Notes

(1) Witten, T. A.; Pincus, P. A. *Macromolecules* **1986**, *19*, 2509–2513.
(2) Russel, W. B.; Saville, D. A.; Schowalter, W. R. *Colloidal Dispersions*; Cambridge University Press: Cambridge, UK, 1989.
(3) Forsman, J. *Curr. Opin. Colloid Interface Sci.* **2006**, *11*, 290–294.
(4) Podgornik, R.; Licer, M. *Curr. Opin. Colloid Interface Sci.* **2006**, *11*, 273–279.
(5) Arya, G. *J. Phys. Chem. B* **2009**, *113*, 15760–15770.
(6) van Opheusden, J. H. J. *J. Phys. A: Math. Gen.* **1988**, *21*, 2739–2751.
(7) Podgornik, R. *J. Phys. Chem.* **1992**, *96*, 884–901.
(8) Podgornik, R. *J. Chem. Phys.* **2003**, *118*, 11286–11296.
(9) Huang, H.; Ruckenstein, E. *Adv. Colloid Interface Sci.* **2004**, *112*, 37–47.
(10) Huang, H.; Ruckenstein, E. *Langmuir* **2006**, *22*, 3174–3179.
(11) Borukhov, I.; Andelman, D.; Orland, H. *J. Phys. Chem. B* **1999**, *103*, 5042–5057.
(12) Akesson, T.; Woodward, C.; Johnsson, B. *J. Chem. Phys.* **1989**, *91*, 2461–2469.
(13) Miklavic, S. J.; Woodward, C. E.; Jonsson, B.; Akesson, T. *Macromolecules* **1990**, *23*, 4149–4157.
(14) Granfeldt, M. K.; Jonsson, B.; Woodward, C. E. *J. Phys. Chem.* **1991**, *95*, 4819–4826.
(15) Sjostrom, L.; Akesson, T. *J. Colloid Interface Sci.* **1996**, *181*, 645–653.
(16) Dzubiella, J.; Moriera, A. G.; Pincus, P. A. *Macromolecules* **2003**, *36*, 1741–1752.
(17) Turesson, M.; Forsman, J.; Akesson, T. *Langmuir* **2006**, *22*, 5734–5741.
(18) Muhlbacher, F.; Schiessel, H.; Holm, C. *Phys. Rev. E* **2006**, *74*, 031919.
(19) Korolev, N.; Lyubartsev, A. P.; Nordenskiold, L. *Biophys. J.* **2006**, *90*, 4305–4316.
(20) Guldbrand, L.; Jonsson, B.; Wennerstrom, H.; Linse, P. *J. Chem. Phys.* **1984**, *80*, 2221–2228.
(21) Zhao, B.; Brittain, W. J. *Prog. Polym. Sci.* **2000**, *25*, 677–710.
(22) Marsaglia, G. *Ann. Math. Stat.* **1972**, *43*, 645–646.
(23) Glotzer, S. C.; Solomon, M. J. *Nat. Mater.* **2007**, *6*, 557–562.
(24) Aknora, P.; Liu, H.; Kumar, S. K.; Moli, J.; Li, Y.; Benicewitz, B. C.; Schadler, L. S.; Acehan, D.; Panagiotopoulos, A. Z.; Pryamitsyn, V.; Ganesan, V.; Ilavsky, J.; Thiyagarajan, P.; Colby, R. H.; Douglas, J. F. *Nat. Mater.* **2009**, *8*, 354–359.
(25) Debye, P. W.; Huckel, E. *Phys. Z.* **1923**, *24*, 185–206.
(26) McQuarrie, D. A. *Statistical Mechanics*; University Science Books: Sausalito, CA, 2000.
(27) Frenkel, D.; Smit, B. *Understanding Molecular Simulation: From Algorithms to Applications*; Academic Press: San Diego, CA, 2002.
(28) Siepmann, J. I.; Frenkel, D. *Mol. Phys.* **1992**, *75*, 59–70.
(29) Frenkel, D.; Mooij, G. C. A. M.; Smit, B. *J. Phys.: Condens. Matter* **1992**, *4*, 3053–3076.
(30) de Pablo, J. J.; Laso, M.; Suter, U. W. *J. Chem. Phys.* **1992**, *96*, 2395–2403.
(31) Striolo, A.; Egorov, S. A. *J. Chem. Phys.* **2007**, *126*, 014902.
(32) Egorov, S. A. *J. Chem. Phys.* **2008**, *129*, 064901.
(33) Smith, G. D.; Bedrov, D. *Langmuir* **2009**, *25*, 11239–11243.
(34) Jayaraman, A.; Schweizer, K. S. *Macromolecules* **2009**, *42*, 8423–8434.
(35) Nykypanchuk, D.; Maye, M. M.; van der Lelie, D.; Gang, O. *Nature* **2008**, *451*, 549–552.
(36) Kegler, K.; Konieczny, M.; Dominguez-Espinosa, G.; Gutsche, C.; Salomo, M.; Kremer, F.; Likos, C. N. *Phys. Rev. Lett.* **2007**, *100*, 118302.
(37) Moreira, A. G.; Netz, R. R. *Eur. Phys. J. E* **2002**, *8*, 33–58.

JP1029085